Reduced Order Modeling in Control of Open Cavity Acoustics

D. M. Bortz, A. D. Rubio, H. T. Banks, A. B. Cain, and R. C. Smith
Center for Research in Scientific Computation
North Carolina State University
Raleigh, North Carolina

July 19, 2000

Abstract

Aircraft with internal carriage of weapons or surveillance systems require active control strategies to limit high amplitude open bay acoustic resonances and to facilitate optimization of structure requirements and weapon/surveillance reliability. This paper focuses on communicating an investigation of the use of numerical simulation combined with Proper Orthogonal Decomposition (POD) model reduction methods to optimize an active control system for aircraft open cavity applications. Issues addressed include characterizing shear layer and wake resonant responses, optimal steady blowing rates, the effect of open loop harmonic perturbations, use of POD for post-processing data to reduce storage requirements, and the use of the Nelder-Mead optimization procedure. Comparison of the wake and shear layer responses reveals why a wake response in aircraft is undesirable. This study has focused primarily on a freestream flow at M=0.85 with a cavity of aspect ratio $l/d = 4.5$. The results include the use of steady blowing injection up to M = 0.9 and harmonic forcing perturbations ranging in amplitude from M=0.005 to M=0.45. In the parameter space examined, fluid displacement had the largest effect. The best observed forcing reduced the buffet loading metrics by approximately 17 db.

1 Introduction

When fluid at high speed flows over an open cavity, large acoustic pressure fields inside the cavity are generated by fluid/structure interactions at the downstream end of the cavity. In the case of an airplane, acoustic waves are created in wheelwells during takeoff and landing, and in weapon and/or surveillance bays during flight. Pressure fluctuations can potentially be high enough to damage stored instrumentation or structures (see for instance [15]). This increases the importance of attenuating the pressure field created within the cavity. In order to

succeed in systematic noise reduction, it is necessary to employ a computational model that captures the essential features of the physical process.

A number of authors have studied the physical mechanism that includes the acoustic waves along with different means to control it. These efforts have involved a variety of cavity shapes and Mach numbers. It is now known that this physical mechanism results in different characteristics depending on the ratio length/depth (l/d) of the cavity. In this regard, a cavity is usually classified as *shallow* or *deep* depending on whether its ratio l/d is greater or less than 2, respectively. In our considerations here (a cavity with $l = 18$ in, $d = 4$ in) we investigated a shallow cavity.

As described in [14], experiments by Rossiter led to a semi-empirical formula to determine the Strouhal number S, a nondimensional cavity resonance frequency

$$S = \frac{f_m l}{U} = \frac{m - \alpha}{M + 1/k}, \tag{1}$$

where M is the mach number, f_m is the frequency, m is the frequency mode number, $k = 0.57$ (a constant related to the disturbance convection speed), U is the freestream velocity, and α is an empirical constant that takes into account the phase difference between the upstream arrival of the acoustic wave and the subsequent shedding of a vortex. The f_m's are the Rossiter frequencies, which correspond to the shear layer (natural Rossiter) mode oscillations. It is important to note that Rossiter's formula assumes the speed of sound inside the cavity to be identical to the speed of sound in the freestream. Therefore, Heller et al. [14] proposed a slight modification to Rossiter's formula that considers the sound speed in the cavity to be nearly equal to the stagnation speed of sound

$$\frac{f_m l}{U} = \frac{m - \alpha}{(M/\{1 + [(\gamma - 1)/2]M^2\}^{1/2}) + 1/k}, \tag{2}$$

where γ is the ratio of specific heats. They found that the estimated error for the predicted values of f_m is $\pm 10\%$ for cavities with $l/d \geq 4$ and greater for cavities with $l/d < 4$. This model has been experimentally studied and for certain regimes verified in [15], [28], [25], and [26].

In [15], H. H. Heller and D. B. Bliss considered a shallow cavity for analysis and experiments. They described the fluid/cavity interaction as a six step feedback loop where instabilities of the shear layer caused a mass addition/removal process at the cavity downstream end. They predicted the mode shapes and amplitudes and implement suppression techniques to reduce them. In [7], Cain, Bower, McCotter, and Romer considered the cases of supersonic and sub-sonic/transonic flow and gave a classification of the flow type along with the corresponding pressure mode shapes for each case. They focused on the case of an "open cavity flow" consisting of cavities satisfying the condition $l/d < 10$, and described the problem as a four-step process where each step was modeled and used to develop a code for modeling. In [26], Rockwell and Nausdacher considered three different perspectives on what originates and sustains the oscillations in the cavity. They discussed the physics characteristics and

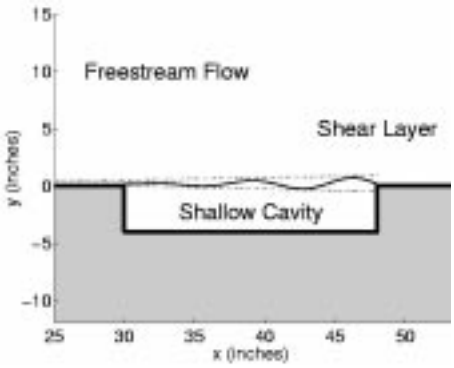

Figure 1: Two dimensional open shallow cavity.

mathematical models for the frequencies and amplitudes in each case. In their paper they presented an extensive summary and comparison of efforts prior to 1978 in terms of analysis, attenuation means, and experimental results.

Here we present computational results for the fluid/structure interactions from a flow over a two-dimensional shallow cavity as depicted in Figure 1 with $2 < l/d < 10$. In this case the fluid-induced oscillation process begins when a boundary layer separates at the upstream end of the cavity, creating an unstable wave. This wave propagates and amplifies downstream across the top of the cavity, where it interacts with the structure, generating an acoustic field. The acoustic wave then propagates back upstream inside the cavity until it reaches the upstream end, feeding the disturbances in the shear layer (see e.g., [7],[15], [26]). In most of the efforts to date, the authors consider a linear model along with semi-empirical formula that predicts modal frequencies (see [7], [15], [26], [28]).

Within an open cavity on an aircraft, sonic resonances in excess of 180 db are possible. Clearly it is desirable to attenuate these waves so as to prevent damage to the aircraft and its payload. Three-dimensional numerical simulations of this phenomena, while more representative of the physics, are computationally prohibitive for design purposes. Fortunately, a two-dimensional simulation does contain sufficient information to yield insight into the physics and is feasible with current computational capabilities. However, to gain the necessary resolution for simulating the high Reynolds number cavity acoustics, we needed to use an approximately 36,000 point grid and run the simulation for approximately 20,000 timesteps to stabilize the flow. After stabilization an additional 4,500 timesteps were needed for the POD calculation described below(a typical timestep is 4×10^{-6} seconds). Unfortunately, each solution snapshot (in time) requires approximately 1.4 megabytes of memory, thus incurring large storage requirements for each simulation run. Therefore, while studying this cavity acoustic phenomena, it became necessary to find a more frugal way to represent the simulation data. This motivated our use of Proper Orthogonal Decomposi-

tion (POD) reduced order methods in carrying out computations for our control problem. Following a description of the full scale numerical method in Section 2, the method and the control problem are described in detail in Sections 3 and 4 below. A description of the simulation approach we used is given in the next section. In concluding this section, we give a few further comments on previous research in the area of cavity acoustics and control.

In summary, a major advance in research on flow over an open cavity was realized in the work of Rossiter (1964)[27] who characterized the modal frequency response for sub-sonic and transonic flows. Since that time many researchers have refined current understanding of the phenomena. While we do not wish to give a comprehensive review, the authors wish to acknowledge the benefit of some of the previous work on prediction and understanding of cavity dynamics and control. These include the already mentioned fundamental advances by Heller and Bliss (1975)[15], frequency and amplitude prediction by Smith and Shaw (1975) [34], modeling by Tam and Block (1978)[36], fundamentals of shear layer feedback loops by Rockwell (1982)[25], fundamental shear layer behavior by Ho and Huerre (1984)[16], advances to modern aircraft application and control by Shaw (1982, 1998)[29][30], challenges to resonant control of experiments by Gharib (1987)[13], issues on nonlinearity by Keefe (1991)[18], challenges in simulation of resonant control Fuglsang and Cain (1992)[12], the wake/shear layer mode switching studies of Colonius et al. (1999)[10], turbulence model advances implemented by Mani and Ota (1999)[20].

Other examples of recent work on cavity acoustics include the papers of Banks et al. (1999)[3], Cain et al. (1999)[6], Cattafesta et al. (1999)[8], Chokani and Lamp (1999)[9], Jacob et al. (1999)[17], Raman et al. (1999)[23], Shaw and Northcraft (1999)[31], Stanek et al. (1999)[35], Arunajatesan et al. (2000)[1], and Williams et al. (2000)[37].

2 A Computational Control Approach

The basis of our control computations involve numerous simulations with non-trivial inputs to alter the flow. We first describe the simulation techniques employed.

2.1 Simulations

Low dissipation, high accuracy schemes with appropriate data densities are required for efficient simulations that accurately reflect the physical behavior of flow over an open cavity. We used the computational aerospace flow code WIND, developed by the NPARC Alliance (a national consortium led by NASA and the Air Force whose purpose is to develop and maintain a specific computational fluid dynamics tool) [22]. For our computational investigations, we have employed third order Runge-Kutta time integration and fifth order spatially refined simulations while using the full Navier-Stokes equations for compressible fluids with turbulence. To better understand the simulation results, time series,

Fourier transforms of time series data, and snapshots of vorticity and pressure fields were generated and monitored. The boundary layer turbulence upstream and downstream of the cavity is modeled by the Spalart-Allmaras model using wall functions for efficiency (see Mani and Ota, 1999)[20] and the flow in the cavity region is computed as a direct numerical simulation in two dimensions.

The choice of numerical schemes (third order Runge-Kutta and fifth order upwind biased) for this work is based on the benchmark problem studies given in Cain and Bower (1995)[5]. In our studies we first contrasted shear layer mode behavior with wake mode behavior. The wake mode occurs for upstream boundary layers that are very thin relative to the cavity length (see Colonius et al., 1999)[10]. Attempts to control the wake mode with forcing (as described below) met with limited success; this result is consistent with the experiments of Gharib (1987)[13] and the simulations of Fuglsang and Cain (1992)[12], both of which addressed wake mode response. Therefore, the primary focus of the investigations reported on below was the shear layer or natural Rossiter mode response both without forcing and with a search for optimized forcing.

2.2 Grid structure, size, forcing and boundary issues

The cavity we considered was 18 inches long by 4 inches deep. The computational domain extended 30 inches upstream from the cavity and 52 inches downstream from the cavity to help maintain flow quality. Numerical damping was applied locally near the upstream, downstream, and freestream boundaries to limit the influence of reflected waves. We used zonei3g (a program used to generate grids for WIND) to create a 3 zone Cartesian grid of approximately 36,000 grid points as depicted in Figure 2. The grid was constructed to limit cell to cell size variations. The Reynolds number was reduced from 1839.71 to 613.104 by lowering the freestream pressure by 1/3. This reduction in Reynolds number means that molecular viscosity dominates the numerical dissipation to produce a meaningful physical response. The introduction of mean and harmonic blowing was through a 60 degree angled slot at the upstream corner of the cavity as depicted in Figure 3. This choice of forcing location avoided the forcing crossing a zone boundary that might produce non-physical influences.

3 Results

3.1 Characteristics of wake and shear layer modes

Figure 4 characterizes the calculated pressure time history for the shear layer and wake modes. The pressure was recorded as a function of time on the downstream cavity wall very near the outer corner as depicted in Figure 5. Using the FFT of the pressure time history, Table 1 allows a comparison between the first 8 modes of oscillation of the numerical simulation with the first 8 natural Rossiter modes. While not perfect, the simulation frequencies for most of the modes are close to those calculated using (2). Additionally, the percent differences are close to

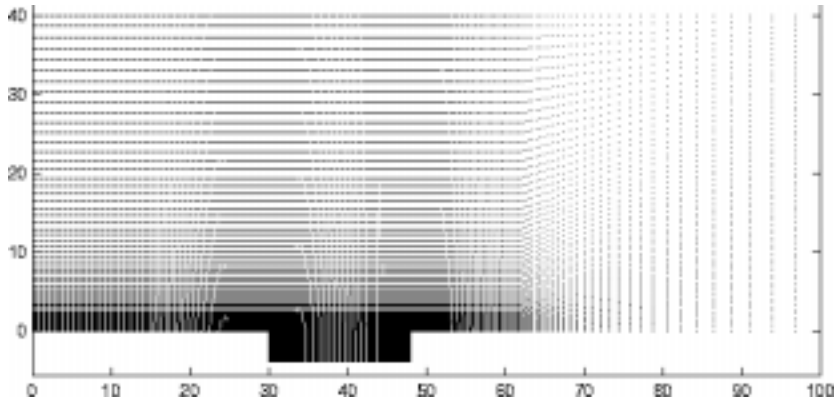

Figure 2: Two dimensional cavity grid generated by zonei3g on an SGI.

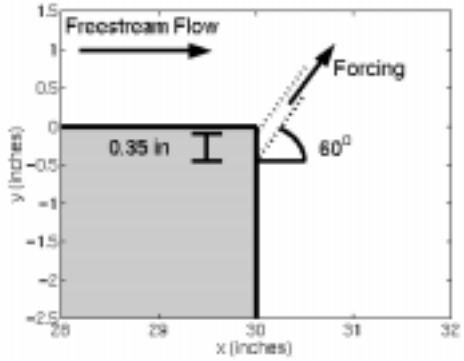

Figure 3: The location of the mean blowing and harmonic blowing slot indicated at the upstream cavity edge.

mode	Rossiter	No Forcing	% difference
1	176.0	370.8	52.5
2	410.6	492.3	14.6
3	645.2	620.2	4.0
4	879.8	856.7	2.7
5	1114.4	1125.3	1.0
6	1349.1	1355.5	0.5
7	1583.7	1489.8	6.3
8	1818.3	1994.9	8.9

Table 1: Comparison of natural Rossiter frequencies and frequencies calculated from the pressure time history taken at the downstream wall.

those predicted by [14] for the higher frequencies, thus lending more weight to the claim that our simulation is a good representation of the dynamics.

It is important to notice that the total pressure variation or buffet loading is much greater for the wake mode. Also the average pressure of the wake mode is much greater, resulting in significantly more drag on an aircraft. Many of the figures in this paper focus on an unsteady pressure or "buffet loading" measure. This unsteady loading metric is essentially an acoustic source measure. It is thus anticipated that reducing the buffet loading metric will amount to beneficial acoustic suppression. Figures 6 and 7 illustrate the significantly different vortical behavior of the shear layer and wake mode responses.

The shear layer mode behavior in Figure 6 is typical and depicts the shear layer bridging the cavity with modest Kelvin-Helmholtz instabilities creating harmonic oscillations in the cavity. In contrast to the shear layer mode, the wake mode response depicted in Figure 7 is characterized by large eruptions of vortical fluid leaving the cavity, and large regions of freestream flow impinging on the downstream wall, creating the high pressure signature. A detailed series of snapshots of the vorticity contours of the wake mode evolution depicts that the shear layer begins to roll up just inside the cavity. This original concentration of vorticity continues to be fed by the upstream boundary layer until it grows sufficiently large to interact with the downstream wall. This interaction is of such a nature that the large concentration of vorticity is ultimately ejected into the freestream. Colonius et al. (1999)[10] performed high-resolution direct numerical simulations with two-dimensional laminar flow for Reynolds numbers of 30-80, based on the shear layer's momentum thickness. They determined that a criterion predicting wake versus shear layer mode response could be given in terms of the ratio of the thickness of the oncoming shear layer to the cavity length. They observed the switch from shear layer mode to wake mode at ratio of cavity length to momentum thickness of between 50 and 100. In our studies the momentum thickness Reynolds number of the upstream boundary layer has been varied between 200 and 600 and the switching between shear layer/wake modal responses is consistent with that observed by Colonius et al. [10].

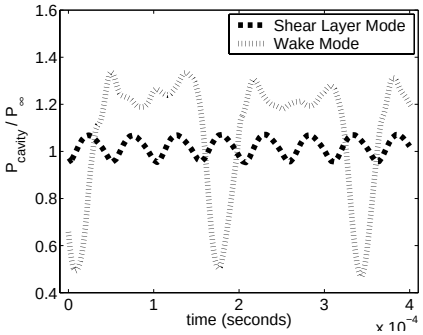

Figure 4: Traces of the time history of pressure on the downstream corner of the wall over several periods of natural oscillations.

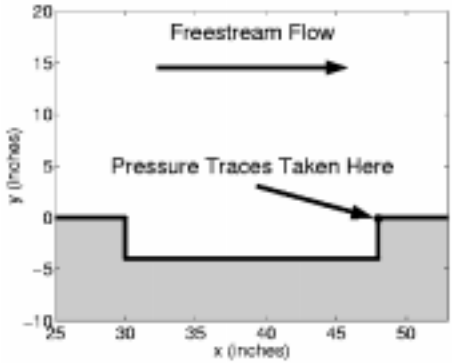

Figure 5: The location from which pressure measurements shown in Figures 4 and 15 were taken.

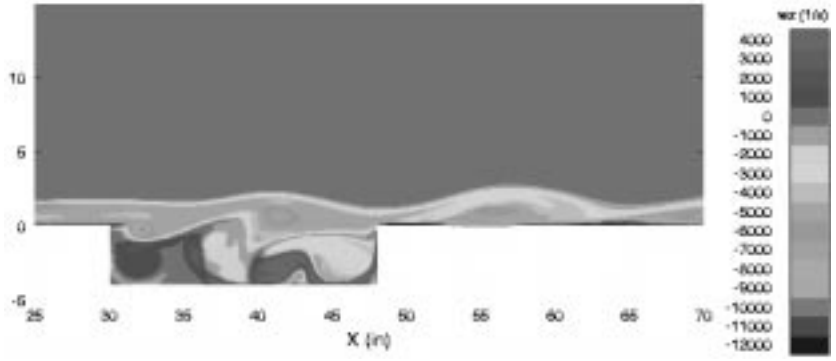

Figure 6: Vorticity contours in a snapshot of the fifth order spatial simulation of the shear layer mode behavior.

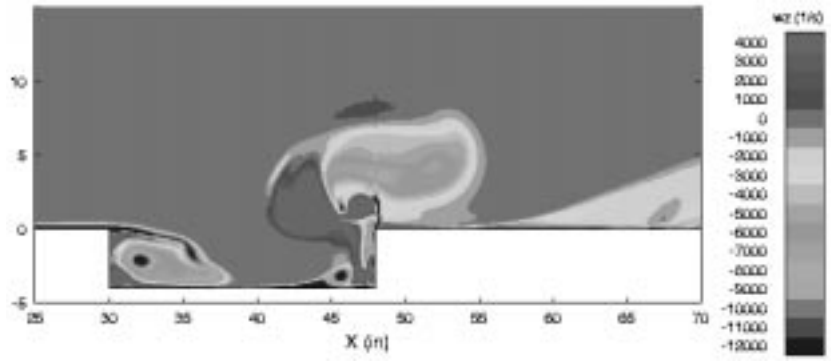

Figure 7: Vorticity contours in a snapshot of the fifth order spatial simulation of the wake mode behavior.

3.2 Forced Cavity Simulations

All simulations reported on here were for a cavity of aspect ratio (l/d) of 4.5 with a freestream flow of Mach 0.85. As depicted in Figure 3, a slot at the upstream edge of the cavity, of cross sectional width less than 1/20 of the cavity depth, at an angle of 60 degrees to the oncoming freestream flow, was used to inject mean blowing and unsteady forcing into the cavity boundary layer. Unsteady disturbances composed of a time-mean flow plus a harmonic perturbation of an amplitude up to the level of the mean blowing were studied. The injected blowing disturbances had velocity amplitudes and harmonic amplitudes ranging from Mach 0.005 to 0.9. To assess the effect of forcing on cavity instability, the integral over the solid boundaries of the square of the difference between the time mean pressure and the instantaneous pressure was used to form metrics of the buffet loading on the upstream wall, downstream wall, and the cavity floor (or ceiling), respectively. More precisely, our metric for the buffet loading BFL was defined as

$$\text{BFL} = \frac{1}{p_\infty} \left\{ \frac{1}{|T||D|} \int_{t \in T} \int_{x \in D} |p(t,x) - \bar{p}(x)|^2 \, dx \, dt \right\}^{\frac{1}{2}} , \tag{3}$$

where the quantities used are given by the following: $p(t,x)$ = pressure at time t and position x, p_∞ = freestream pressure, $\bar{p}(x)$ = average pressure, T = time interval of interest, $|T|$ = length of time T, D = domain of interest, and $|D|$ = length of domain D.

An overview of the cases examined can be observed in Figure 8. The x-axis in this figure is the sum of the harmonic and steady blowing amplitudes which is the maximum forcing amplitude realized in each run. The no forcing case is identified to provide a reference point for the other cases. These included a range of frequencies and ratios of harmonic amplitude to mean blowing levels. Note that use of forcing disturbances less than M = 0.2, for the computational configuration examined here, dramatically increases the buffet loading.

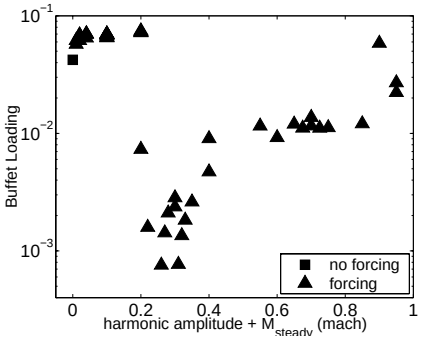

Figure 8: A simple presentation of the cases examined with buffet loading expressed as a function of the sum of mean and harmonic forcing Mach number.

The cluster of cases of low harmonic plus steady blowing in the upper left of Figure 8 consists solely of cases where the steady blowing was zero. Thus, the fact that we were not able to reduce the buffet loading by using small amplitude harmonic blowing suggests that the effective use of open loop control (with small amplitude disturbances) will be a challenge. The rise in buffet loading at steady blowing values higher than M = 0.8 is believed to be due to the effect of strong entrainment flows that occur at high blowing rates. It is also possible that the boundary layer is separating from the wall upstream of the cavity, which would also generate this effect. Figures presented below will reveal that modest blowing gently lifts the shear layer over the downstream cavity corner and softens the interactions of shear layer vortical instabilities with the corner.

Figure 9 isolates the effect of mean blowing level on the buffet loading level by fixing the harmonic perturbation level at M=0.25 with a frequency of 361 Hz (90% of the second Rossiter mode) and then varying the mean blowing rate. It is readily apparent that there is a flat trough for a mean blowing level ranging from M=0.3 to M=0.6. It is believed that this level trough is due to the harmonic forcing influence and that the level may come down with lower harmonic amplitudes. Figure 10 depicts various harmonic forcing levels for 3 mean blowing levels, all with harmonic frequency of 361 Hz. The loading metric decreases as harmonic levels are decreased until, at small harmonic levels the loading increases as the harmonic forcing goes to zero. Many of the experimental studies to date have focused on the issue of different forcing frequencies. Our simulations exhibit very important significant differences with respect to experiments and additionally provide some complementary information on open loop forcing as well. Note that all cases in Figure 11 have harmonic blowing amplitude equal to the mean blowing level ranging from M=0.005 to M=0.45.

In Figure 11 a substantial range of frequencies of harmonic excitation exhibits limited improvement in the buffet loading for these combinations of forcing. The relevance of the frequencies examined, is given a context by the indicated first two Rossiter frequencies. Figure 12 illustrates the behavior of a given

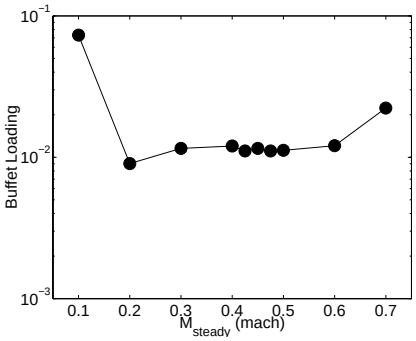

Figure 9: Buffet loading metric as a function of the mean blowing level for a harmonic forcing level of M=0.25 at a frequency of 90% of the second Rossiter frequency (361 Hz).

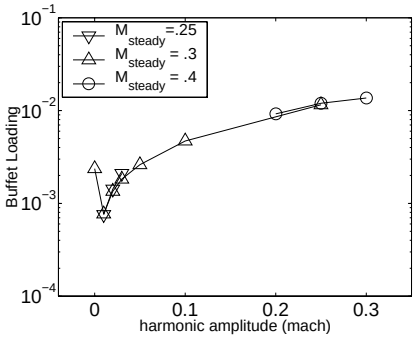

Figure 10: Behavior of the buffet loading metric at several harmonic forcing amplitudes for mean blowing levels of M=0.3 and M=0.4 and frequency of Figure 9.

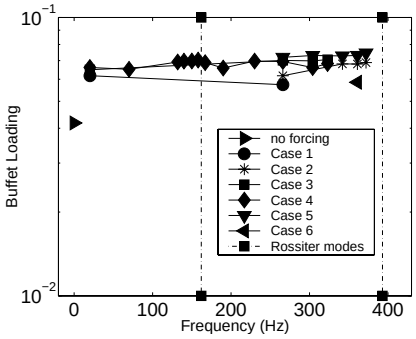

Figure 11: Buffet loading level at many frequencies with the harmonic forcing level equal to the mean blowing for Case 1, M= 0.005; Case 2, M=0.01; Case 3, M=0.02; Case 4, M=0.05; Case 5, M=0.1; and Case 6, M=0.45.

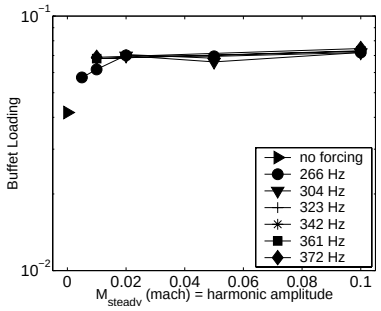

Figure 12: Buffet loading metric for several frequencies with harmonic forcing levels equal to the mean blowing Mach number.

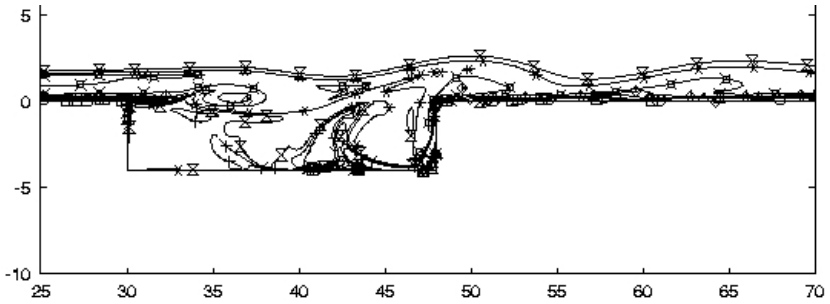

Figure 13: Contours of vorticity for a very weakly forced flow. The freestream Mach number is M=0.85. The mean blowing and harmonic forcing amplitudes are both M=0.01 and the frequency of forcing is 90% of the second Rossiter frequency (361 Hz). The contours levels are in increments of vorticity jumps of 2000/sec.

harmonic frequency over a range of amplitudes of harmonic forcing and mean blowing. Note that in all cases in Figure 12, the mean blowing Mach number is equal to the harmonic perturbation amplitude. It is also important to observe in Figures 11 and 12, that the minimal buffet loading is achieved with *no blowing*, that is, without any control.

The behavior illustrated in Figures 8 through 12 suggests that open loop harmonic forcing is somewhat limited in reducing the buffet loading in these simple two-dimensional numerical simulations. To gain a better understanding of the benefit of the mean blowing we turn to the visualization in Figures 13 and 14. The conditions for Figure 13 are for an amplitude of harmonic forcing and mean blowing of Mach 0.01. The results are very similar to those for no forcing except that the disturbances are regularized instead of random. Figure 14 exhibits a suboptimal reduced buffet loading levels relative to the unforced simulations.

This acoustic suppression depicted in Figure 14 was generated by mean blowing at a Mach number of 0.4 with a harmonic forcing frequency of 361 Hz and

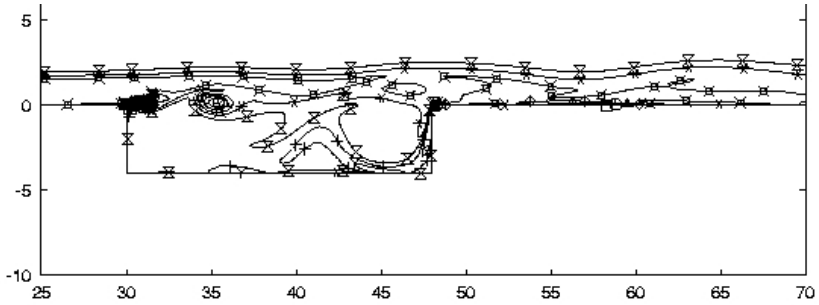

Figure 14: Contours of vorticity for a suboptimal forced flow. The freestream Mach number is M=0.85. The mean blowing level is M=0.4 and harmonic forcing amplitude is M=0.2 and the frequency of forcing is 90% of the second Rossiter frequency (361 Hz). The contour levels are in increments of vorticity jumps of 2000/sec.

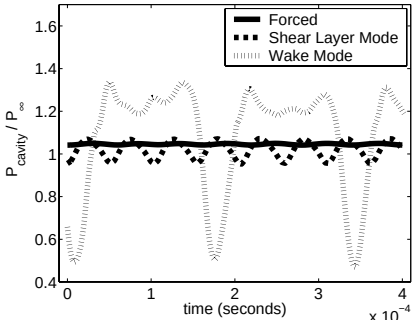

Figure 15: Traces of the times history of the pressure on the downstream corner of the wall.

an amplitude of Mach 0.2. Both of these simulations show the forcing-induced development of the Kelvin-Helmholtz instability. However, in the highly suppressed case depicted in Figure 14, the mean blowing gently raises the perturbed shear layer over the downstream corner and the vortical interactions with the corner are reduced. Another aspect of this effect is illustrated by the stronger gradients of vorticity inside the cavity in Figure 13, indicating strong shear layers and the presence of more dynamic activity in the cavity. Figure 15 depicts the pressure time history of a suboptimally forced ($M_{steady} = 0.25$ Mach and $M_{harmonic} = 0.01$ Mach) case juxtaposed with the shear layer and wake modes with no blowing. Based upon the buffet loading metric, we calculated that this suboptimal forced case was 17.4 db lower than the shear layer mode without blowing.

The discussion has suggested significant differences between the wake mode response, the shear layer mode response, and the optimized forcing case. These

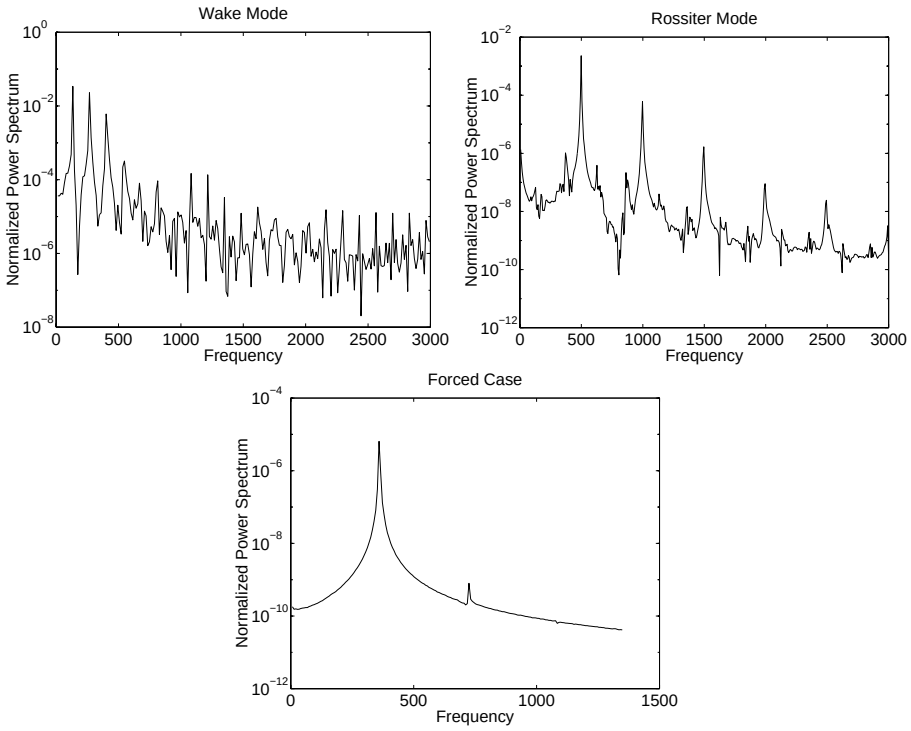

Figure 16: Spectra from the Wake Mode, Rossiter Mode, and Forced ($M_{steady} = 0.25$ Mach, $M_{harmonic} = 0.01$ Mach, 361 Hz) cases.

differences are further emphasized in the corresponding spectra from the three cases. Figure 16 shows the power spectra of all three cases based on fluctuating pressure, normalized by the freestream pressure and determined from a time series of data taken at the downstream corner as shown in Figure 5. The wake mode has larger amplitude oscillations and lower frequency content. Both of these distinguishing features have a detrimental effect on operational reliability and maintenance costs. Clearly, in real designs the wake mode should always be avoided. The shear layer mode response at this Mach number and geometry tends to give a 2nd Rossiter mode as the dominant response. For other Mach numbers and geometries different Rossiter modes may be more important. The case of optimized forcing shows a dramatic reduction in spectral amplitudes and only the forcing frequency and its first harmonic rise above a quiet background. As had been speculated earlier, the steady component of forcing has gently lifted the shear layer above the downstream corner minimizing disturbance interactions with the downstream corner. This reduced interaction lowers the gain of the feedback loop resulting in the very low amplitude, quiet spectrum.

4 Proper Orthogonality Decomposition

In the previous section, we used extensive simulations to suggest that optimal or suboptimal strategies for suppression of acoustic pressure fields in shear layer flows over open cavities may be achieved by an injection of mass (injected flows) at appropriate combinations of mean blowing level and harmonic forcing at certain frequencies. These numerical simulations were made feasible by the use of a model reduction/data reduction technique which we now describe in some detail.

To simplify the post processing and storage of the numerical simulation data we took advantage of the Proper Orthogonal Decomposition (POD) (see [2], [19] for other successful uses of POD in both open loop and closed loop control applications to flow and structural problems). POD is a method for representing elements in a vector field in an L^2 optimal sense. While generally it would be expected that POD methods would be used on vector fields of vectors, for demonstration purposes, we simplified our problem by only examining vector fields of scalar pressure values. However, for this theoretical development we consider a generic vector field $u(t,x)$ satisfying

$$u:\ [0,\infty)\times\Omega\to\mathbb{C},$$

where Ω is some spatial domain with $x\in\Omega$, $\mathbb{C}$ is the complex field, and $0\le t<\infty$.

4.1 Infinite Dimensional Theory

The POD representation of u is a linear combination of some set of basis functions $\{\phi_i\}\in L^2(\Omega)$

$$u(t,x)=\sum_{i=1}^{\infty}a_i(t)\phi_i(x)$$

with

$$a_i(t)=(u(t,\cdot),\phi_i(\cdot))_{L^2} \tag{4}$$

and $(\cdot,\cdot)_{L^2}$ denoting the L^2 inner product.

Clearly it would be ideal to find normalized basis functions $\phi\in L^2(\Omega)$ that solve:

$$\max_{\|\phi\|=1} <(u,\phi)_{L^2}^2>$$

where $<>$ denotes the time average given by

$$<f>=\frac{1}{T}\int_0^T f(t)\ dt\,.$$

The POD method was initially developed for use in modeling stochastic processes, thus T is assumed to be large enough so that the time average converges

(See [4] for a review of the use of the POD method in fluid flow applications). Since we are primarily concerned with steady state oscillations, we have made the same assumption.

By a simple expansion, we obtain

$$< (u,\phi)^2_{L^2} >= \int_\Omega \left(\int_\Omega < u(\cdot,x)\, u^\star(\cdot,x') > \phi(x')dx' \right) \phi^\star(x)dx\,,$$

where $\star$ denotes the complex conjugate.

We denote the integral inside the parenthesis as $R_u(\phi)$, where $R_u : L^2(\Omega) \to L^2(\Omega)$, and note that in maximizing $(R_u(\phi),\phi)_{L^2}$, we will maximize $< (u,\phi)^2_{L^2} >$.

Now, upon examining the R_u mapping we observe that

$$\begin{array}{lcl} (R_u(\phi),\psi)_{L^2} & = & (\phi, R_u(\psi))_{L^2} \text{ for all } \phi,\psi \in L^2\,, \\ (R_u(\phi),\phi)_{L^2} & \geq & 0 \text{ for all } \phi \in L^2\,, \end{array}$$

and thus R_u is a symmetric, positive semi-definite mapping from $L^2(\Omega)$ to $L^2(\Omega)$.

Note further that $(R_u(\phi),\phi)_{L^2}$ will be maximized when ϕ is the eigenfunction corresponding to the largest eigenvalue of R_u. Thus the problem of finding basis functions consists of solving the following eigenvalue problem

$$R_u\phi = \lambda\phi\,, \tag{5}$$

with $||\phi|| = 1$.

Indeed, it is possible to prove that using the eigenfunctions as the basis is in some sense "optimal." Specifically, consider any other basis $\{\psi_i\}$ upon which u is projected

$$u(t,x) = \sum_{i=1}^{\infty} b_i(t)\,\psi_i(x)$$

with

$$b_i(t) = (u(t,\cdot),\psi_i(\cdot))_{L^2}\,. \tag{6}$$

As is proved in [4], for all $n \in \mathbb{N}$,

$$\sum_{i=1}^{n} < a_i\, a_i^\star > = \sum_{i=1}^{n} \lambda_i^2 \geq \sum_{i=1}^{n} < b_i\, b_i^\star >\,, \tag{7}$$

where the $a_i(t)$ are defined in (4) and the $b_i(t)$ are defined in (6).

Therefore, if we assume momentarily that the vector field is a velocity field, we could non-dimensionalize ψ, giving the a_i's units of velocity. Thus we can perceive $\sum_{i=1}^{n} < a_i\, a_i^\star >$ as a "velocity squared" term. Normalizing away the mass implies that this sum of the time averages provides a measure of the energy term.

Thus, among all possible linear decompositions, this eigenfunction representation contains the most "kinetic energy" possible, and thus it is referred to as an optimal basis (in an L^2 sense).

It is crucial to note that the ability to calculate this "kinetic energy" depends on our assumption that the original vector field is a velocity field. If we assume that the vector field is a displacement field, the sum in (7) can be viewed as a "potential energy" term. In reality, the vector field could be any scalar quantity. However, viewing the scalars as velocities leads to the insight that (7) is a kinetic energy-like term, and in practice is referred to as the "kinetic energy" regardless of the units of the original vector field.

4.2 Finite Dimensional Theory

Consider a set of snapshots of the vector field discretized in space and time $\{u(t_1, \bar{x}),\ u(t_2, \bar{x}),\ u(t_3, \bar{x}),\ldots,u(t_n, \bar{x})\}$, with $\bar{x}$ representing the discretization in space.

From [24], if follows that for a hermitian operator with eigenvalues λ_i we have

$$\sum_{i=1}^{\infty} \lambda_i^2 < \infty\,. \tag{8}$$

Thus, as described above, the "kinetic energy" associated with the hermitian operator R_u from (5), can be represented by a sum of squares of its eigenvalues (by (7)). Thus, choosing n large implies that the generated eigenvalues might represent a majority of the "kinetic energy" of the entire system. If this is true, then it is also possible that a large percentage of the "kinetic energy" of the system could be encapsulated within the first few modes, i.e., for m small

$$\%KE = \frac{\sum_{i=1}^{m} \lambda_i^2}{\sum_{j=1}^{n} \lambda_j^2}\,.$$

In practice, we found this to be the case for our system.

We consider (without justification yet) basis elements of the form

$$\phi_i(\cdot) = \sum_{j=1}^{n} \bar{c}_j\, u_j(\cdot)\,, \tag{9}$$

where $\bar{c}$ is an n-dimensional vector of scalars. Substituting this form of basis elements into (5) and expanding, generates the equation

$$\sum_{i,j=1}^{n} \left((u_i,\, u_j)_{L^2}\ \bar{c}_j \right) u_i = \lambda \sum_{i=1}^{n} u_i\, \bar{c}_i\,.$$

After some manipulation, we obtain

$$u^T \left[(u_i,\, u_j)_{L^2} \right] \bar{c} = u^T (\lambda\, \bar{c})\,,$$

and for u non-zero, we again have an eigenvalue problem.

Note that the eigenvalues of the matrix who's (i,j)th element is $[(u_i,\, u_j)_{L^2}]$ are eigenvalues of R_u. In (9), we used $\bar{c}$ to define the ϕ_i's , which are the eigenfunctions of R_u. By the discussion following (7), these ϕ_i's are optimal in an L^2 sense. Therefore, using this linear combination of the snapshots (9) to create the basis functions does generate an optimal basis.

4.3 POD Application to the Cavity Acoustics Simulations

The POD method is a constructive approach for determining basis elements in an efficient manner using N time-dependent snapshots. This section describes the implementation of POD and it's efficacy in reducing the storage requirements for the pressure field.

In practice, choosing N large frequently (in the case of so-called coherence in the snapshot data) yields

$$\sum_{i=1}^{N} \lambda_i \cong \sum_{i=1}^{\infty} \lambda_i < \infty\,.$$

Since we know from (7) that the sum of the eigenvalues is the "kinetic energy" of the system, the finite sum is typically a good approximation of the "total kinetic energy."

We chose to take $N = 101$ (two dominant oscillation cycles) pressure snapshots in time: $\{\bar{p}(t_1,\bar{x}),\, \bar{p}(t_2,\bar{x}),\, \bar{p}(t_3,\bar{x}),\ldots,\bar{p}(t_{101},\bar{x})\}$ where $\bar{x}$ and $\bar{p}$ represent the grid and a 35,739 element vector of pressure values at time t_i respectively. Note that the dimension of $\bar{p}$ corresponds to the number of grid points.

WIND stores the data about the flowfield in a binary file adhering to the NPARC common flow field (cfl) specifications [22]. Since Matlab was the programming language chosen to implement the POD method, a conversion script was written to change the cfl file into a matlab-readable ASCII text file.

Once the pressure field data was imported into Matlab, treating the pressure field as a vector in $\mathbb{R}^{35,739}$, we solved the eigenvalue problem

$$A\,\bar{c} = \lambda\,\bar{c}\,,$$

where A is the (101×101) matrix whose (i,j)th element is $(\bar{p}(t_i,\bar{x}),\, \bar{p}(t_j,\bar{x}))_{L^2}$.

The sorted and normalized magnitudes of the eigenvalues are plotted in Figure 17. Clearly, the magnitude of the eigenvalues decrease rapidly, and as is depicted in Figure 18, the first 4 modes contain 99.9999% of the "energy" in these snapshots. Therefore, we felt that using the first 10 modes would be more than sufficient to capture all the significant information in the system.

Using the coefficients from the eigenvectors $\{\bar{c}_i\}_{i=1}^{101}$, we constructed the basis elements from a linear combination of the snapshots

$$\phi_i(\cdot) = \sum_{j=1}^{101} c_{ij}\, u_j(\cdot) \text{ for } i = 1,\ldots,10\,.$$

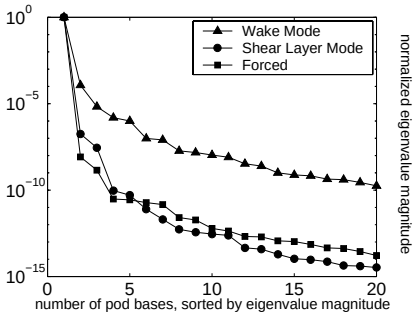

Figure 17: Distribution of normalized amplitudes of POD elements. The wake mode, shear layer mode, and forced case are the same as the cases in Figure 15.

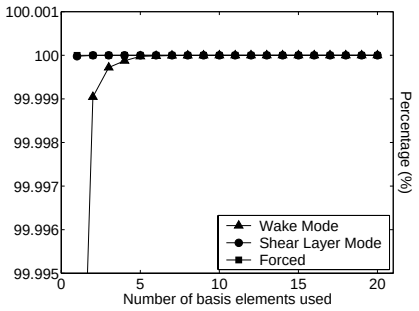

Figure 18: Measure of POD convergence based on relative 'energy' of pressure representation. The wake mode, shear layer mode, and forced case are the same as the cases in Figure 15.

Using WIND to run our simulations, each spatially discretized snapshot requires approximately 2 MB of storage in an ASCII format. Thus to store $N = 100$ snapshots would require 200 MB. Projecting onto the first 10 POD basis elements, these elements and the coefficients for 100 snapshots requires merely 2 MB of storage. Clearly POD is an extraordinarily valuable tool for reducing storage requirements when carrying out simulations and control calculations. We are aware that simply compressing the ASCII data would also save considerable space and present these results to describe the relative merits of POD in the absence of other storage saving mechanisms.

In an attempt to reduce RMS pressure metrics (analogous to buffet loading), we injected air (at the upstream edge of the cavity) at a variety of frequencies, steady blowing amplitudes, and unsteady blowing amplitudes as previously described in Section 3.2. For each set of forcing parameters we have calculated an approximation to the metric described above in (3). The finite dimensional POD-based version of the metric is

$$\mathrm{BFL}_{(M,N)} = \frac{1}{p_\infty} \left\{ \frac{1}{N|D_M|} \sum_{j=1}^{N} \sum_{i=1}^{M} w_i \left| p(t_j, \bar{x}_i) - \bar{p}(\bar{x}_i) \right|^2 \right\}^{\frac{1}{2}}, \qquad (10)$$

where the w_i are the quadrature weights, D_M is a specific set of points representing a subdomain of the spatial grid (e.g., the grid points along the downstream wall of the cavity), and the $\bar{x}_i$ are the M quadrature points in D_M. Note that in the actual calculation of the metric, the reduced POD representations were used for the pressure fields. Since we are more interested in the metrics relative to one another, we used the simple trapezoid method to approximate the integral. The metric was calculated for three distinct sub-domains: the downstream wall, the upstream wall, and the bottom wall (all in the cavity). We found that each of the three metrics were, in general, directly proportional to one another, and thus focused our attention on the downstream wall metric. Varying the frequency did not have as much effect upon the buffet loading metric as varying the steady and unsteady magnitudes. Therefore, we only optimized over the 2D parameter space of steady forcing and unsteady forcing Mach numbers. Using a cubic interpolation over the parameter space, we used Nelder-Mead [21] in an attempt to minimize the downstream metric over the parameter space, where the algorithm converged to a local minimum at $M_{steady} = 0.2805$ Mach and $M_{unsteady} = 0.0111$ Mach. We chose Nelder-Mead because the algorithm does not require the calculation of gradients and tends to work well when optimizing over a low dimensional space.

5 Discussion

5.1 Comparing numerical simulations to experimental data

While numerical simulations are of considerable value for sorting out hypotheses, it is essential to realize that there are potentially very significant differences

between the assumptions used in numerical simulations and laboratory or flight situations. The first major simplification is that of two-dimensional domain cavity simulation. While simulations can be performed which include some aspects of three-dimensionality, a parametric study in three dimensions was computationally prohibitive, given our computational resources. Any simulations of the cavity that include full three-dimensional simulation of the turbulence in the oncoming boundary layer are also computationally prohibitive.

These computational studies were done in the context of a numerically focused study in two dimensions without guidance from experiments. Smith (2000)[34] and Shaw (2000)[32] have both pointed out that cavity simulations performed in three-dimensions often behave significantly different than two-dimensional simulations. One experience related to our two-dimensional approach was that we found that a large number of forcing conditions needed to be examined before finding a benefit of forcing. It is interesting to learn that in early experimental studies, Shaw (2000)[32] examined many forcing conditions finding substantial numbers of cases both with beneficial results and without beneficial results. Thus, in this respect our efforts to find effective controls were commensurate with experimental findings.

Our simulations were done without knowledge of the parameter space used in Shaw's experiments. As a result, the cavity geometry, blowing geometry, and blowing velocities were quite different in Shaw's experiments than in our simulations. In an attempt to compare the experimental and simulation results, a simple engineering forcing parameter is proposed. The parameter is based on the volumetric inflow of the forcing stream per unit width, the freestream velocity and the cavity length. The parameter is $\chi = \frac{V_{in} G_{slot}}{U_\infty L_{cavity}}$, where V_{in} is the vertical component of the blowing velocity, G_{slot} is the effective blowing slot gap, U_∞ is the freestream velocity, and L_{cavity} is the length of the cavity. In the case of the experimental information used here, the blowing flow chokes and the fully expanded blowing velocity was used to compute χ. The experimental values tabulated in Table 2 are those from data provided by Shaw (2000)[32].

Additionally, the fact that the mass flux weighted parameter (χ) range is of the same order of magnitude for the forcing in the experiments and our computations not only supports the validity of a comparison between the two, but also the idea that the primary suppression effect derives from the displacement of the shear layer. This is particularly significant since the momentum parameter for the forcing is 3-15 times larger for the experiment than it is in our computations [32]. It is believed that the experiment did not benefit from forcing in the horizontal injection cases because it essentially amounts to placing an acoustic source inside the cavity. Recall that the simulations seem to indicate that the harmonic forcing at large amplitudes drives the buffet metric (see Figure 9). Finally, while the experimental harmonic forcing velocities are 3-15 times the computational levels, they may not produce the same impact since the geometries are usually quite different.

Data Type	Mass Flow/ Mach Injection	χ
Experimental A	0.3 lbs/sec.	0.0012
Experimental A	0.4 lbs/sec.	0.0016
Experimental A	0.5 lbs/sec.	0.0020
Experimental B	0.3 lbs/sec.	0.0012
Experimental B	0.4 lbs/sec.	0.0016
Experimental B	0.5 lbs/sec.	0.0020
Computational	Mach 0.2	0.0013
Computational	Mach 0.3	0.0020
Computational	Mach 0.4	0.0026
Computational	Mach 0.5	0.0033
Computational	Mach 0.6	0.0040
Computational	Mach 0.7	0.0046

Table 2: Table of blowing parameter values.

6 Conclusions

We conclude with a brief summary of our findings. First, both the shear layer and wake mode responses have been demonstrated computationally in a 2-dimensional setting. Wake modes are very undesirable and understanding them better will help to insure no aircraft designs in the wake mode regime are considered.

Steady blowing can successfully reduce buffeting metrics. Our simulations suggest that the blowing level has an optimal range. The present computations and experiments of Shaw seem to be consistent in the level of blowing that has a beneficial impact. High blowing levels can create an entrainment induced cavity disturbance.

To enable comparison between our simulations and experiments of others, a simple algebraic parameter has been defined. This parameter appears to be useful in relating disparate experiments and computations and providing guidance for optimal (or suboptimal) open loop control.

In addition to steady blowing, the effect of harmonic excitation was examined. Many initial cases at many frequencies and amplitudes revealed no benefit from harmonic excitation. However, eventually we found that small amplitude harmonic forcing in addition to a mean component of blowing provided a suboptimally reduced buffet metric observed in the present investigation. The most significant of these resulted in a 17.4 db reduction.

Proper Orthogonal Decomposition methods provide a valuable tool for post processing. They reduce computation and more importantly reduce storage requirements. Moreover, the POD methodology can be readily incorporated into optimization schemes such as Nelder-Mead to accelerate finding an optimal solution.

7 Acknowledgements

The authors wish to acknowledge the benefit of discussions with Tim Colonius, Ed Kerschen, Val Kibens, Mori Mani, Leonard Shaw, and Dave Williams. Members of the Center for Research in Scientific Computation at North Carolina State University also wish to acknowledge the software support of The Boeing Company. This research was supported in part by the U.S. Air Force Office of Scientific Research grant AFOSR-F49620-98-1-0180 and in part through a GAANN Fellowship to David Bortz under Department of Education grant P200A980801.

References

[1] S. Arunajatesan, N. Sinha, and S. Menon, "Towards Hybrid LES-RANS Computations of Cavity Flowfields," AIAA-2000-0401, January 2000.

[2] H. T. Banks, R.C.H. del Rosario, and R. C. Smith, "Reduced Order Model Feedback Control Design: Numerical Implementation in a Thin Shell Model," CRSC-TR98-27, July, 1998, N. C. State Univ.; IEEE Transactions Auto. Control, to appear.

[3] H. T. Banks, A. D. Rubio, and R. C. Smith, "Modeling Acoustic Fields Generated by Flow Past an Open Cavity," AIAA-99-1913, May 1999.

[4] G. Berkooz, P. Holmes, and J. L. Lumley, "The Proper Orthogonal Decomposition in the Analysis of Turbulent Flows," Annual Review of Fluid Mechanics, Vol. 25, pp 525-539, 1993.

[5] A. B. Cain and W. W. Bower, "Comparison of Spatial /numerical Operators for Duct-Nozzle Acoustics," Proceedings of the ICASE/LaRC Workshop on Bench Mark Problems in Computational Aeroacoustics, NASA Conference Publication 3300, May 1995.

[6] A. B. Cain, W. W. Bower, and F. McCotter, "Modeling and Prediction of Weapon Bay Acoustic Amplitude and Frequency," P.O. P6110-5016, Tech Report, submitted to VBDA, Inc., February 1996.

[7] A. B. Cain, W. W. Bower, F. McCotter, and W. W. Romer, "Quick Turnaround Prediction of Weapons Bay Cavity Acoustic Resonance," AIAA-99-1899, May 1999.

[8] L. Cattafesta III, D. Shukla, S. Garg, and J. Ross, "Development of an Adaptive Weapons-Bay Suppression System," AIAA-99-1901, May 1999.

[9] N. Chokani and A. Lamp, "Computation of Unsteady Incompressible Cavity Flow with Pulsed Jet Control," AIAA-99-1914, May 1999.

[10] T. Colonius, A. Basu, and C. Rowley, "Numerical Investigation of Flow Past a Cavity," AIAA-99-1912, May 1999.

[11] T. Colonius, Private communication, September 1999.

[12] D. F. Fuglsang and A. B. Cain, "Evaluation of Shear Layer Cavity Resonance Mechanisms by Numerical Simulation," AIAA 92-0555, January, 1992.

[13] M. Gharib, "Response of the Cavity Shear Layer Oscillations to External Forcing," AIAA Journal, Vol. 25, No. 1, pp. 43-47, 1987.

[14] H. H. Heller, D. G. Holmes, and E. E. Covert, "Flow Induced Pressure Oscillations in Shallow Cavities," Journal of Sound and Vibration, Vol. 18, No. 4, 1971, pp. 545-553.

[15] H. H. Heller and D. B. Bliss, "The Physical Mechanism of Flow Induced Pressure Fluctuations in Cavities and Concepts for Suppression," AIAA 2nd Aeroacoustics Conference, Paper 75-491, March 1975.

[16] C. M. Ho and P. Huerre, "Perturbed Free Shear Layers," Annual Review of Fluid Mechanics, Vol. 16, 1984, pp. 365-424.

[17] M. Jacob, V. Gradoz, A. Louisot, D. Juve, S. Guerrand, "Comparison of Sound Radiated by Shallow Cavities and Backward Facing Steps," AIAA-99-1892, May 1999.

[18] L. Keefe, "Multiple Solutions. A Barrier to Flow Control?," Presented at the Forty-Fourth Annual Meeting of the Division of Fluid Dynamics of the American Physical Society, Scottsdale AZ, Nov. 1991.

[19] H. V. Ly and H. T. Tran, "Proper Orthogonality Decomposition for Flow Calculations and Optimal Control in a Horizontal CVD Reactor," CRSC-TR98-13, March 1998, N. C. State Univ.; Quarterly of Applied Mathematics to appear.

[20] M. Mani, and D. Ota, "A Compressible Wall Function for Steady and Unsteady Flow Applications," AIAA 99-3216, June 1999.

[21] J. A. Nelder and R. Mead, "A Simplex Method for Function Minimization," Comput. J., 7(1965), pp. 308-313.

[22] NPARC http://www.arnold.af.mil/nparc/

[23] G. Raman, S. Raghu, and T. Beninc, "Cavity Resonance Suppression Using Miniature Fluidic Oscillators," AIAA-99-1900, May 1999.

[24] F. Riesz and B. S. Nagy, "Functional Analysis," Ungar, New York, 1955.

[25] D. Rockwell, "Invited Lecture: Oscillations of Impinging Shear Layers," AIAA 82-0047, January 1982.

[26] D. Rockwell and E. Nausdacher, "Review: Self-Sustaining Oscillations of Flow Part Cavities," Journal of Fluids Engineering, Vol 100, pp 152-165, 1978.

[27] J. E. Rossiter, "Wind Tunnel Experiments on the Flow Over Rectangular Cavities at Subsonic and Transonic Speeds," Royal Aircraft Establishment, TR No. 64307, October 1964.

[28] R. L. Sarno and M. E. Franke, "Suppression of Flow-Induced Pressure Oscillations in Cavities," Journal of Aircraft, Vol 31, pp 90-96, 1994.

[29] L. L. Shaw, "Full Scale Flight Evaluation of Suppression Concepts for Flow-Induced Fluctuating Pressures in Cavities," AIAA 82-0329, January 1982.

[30] L. L. Shaw, "Active Control for Cavity Acoustics," AIAA 98-2347, June 1998.

[31] L. L. Shaw, and S. Northcraft, "Closed Loop Active Control for Cavity Acoustics," AIAA-99-1902, May 1999.

[32] L. L. Shaw, private communication, March 2000.

[33] B. Smith, private communication, January 2000.

[34] D. L. Smith and L. L. Shaw, "Prediction of the Pressure Oscillations in Cavities Exposed to Aerodynamic Flow," AFFDL-TR-75-34, October 1975.

[35] M. Stanek, R. Sinha, and R. Birkbeck, "Acoustics-Compatible Active Flow Control for Optimal Weapons Separation," AIAA-99-1911, May 1999.

[36] C. K. W. Tam and P. J. W. Block, "On the Tones and Pressure Oscillations Induced by Flow over Rectangular Cavities," Journal of Fluid Mechanics, Vol. 89. Part 2, pp. 373-399, 1978.

[37] D. R. Williams, D. Fabris, K. Iwanski, and J. Morrow, "Closed-Loop Control in Cavities with Unsteady Bleed Forcing," AIAA-2000-0470, January 2000.